Published in final edited form as:
Cancer Res. 2014 December 15; 74(24): 7583–7598. doi:10.1158/0008-5472.CAN-14-1235.

Oncogene pathway activation in mammary tumors dictates [^{18}F]-FDG-PET uptake

James V. Alvarez[1,3], **George K. Belka**[1,3], **Tien-chi Pan**[1,3], **Chien-Chung Chen**[1,3], **Eric Blankemeyer**[4], **Abass Alavi**[4], **Joel Karp**[4], and **Lewis A. Chodosh**[1,2,3,*]

[1]Department of Cancer Biology, Perelman School of Medicine at the University of Pennsylvania, Philadelphia, PA 19104, USA

[2]Department of Medicine, Perelman School of Medicine at the University of Pennsylvania, Philadelphia, PA 19104, USA

[3]Abramson Family Cancer Research Institute, Perelman School of Medicine at the University of Pennsylvania, Philadelphia, PA 19104, USA

[4]Department of Radiology, Perelman School of Medicine at the University of Pennsylvania, Philadelphia, PA 19104, USA

Abstract

Increased glucose utilization is a hallmark of human cancer that is used to image tumors clinically. In this widely used application, glucose uptake by tumors is monitored by positron emission tomography (PET) of the labeled glucose analog F-18-2-fluoro-2-deoxyglucose (^{18}F-FDG). Despite its widespread clinical use, the cellular and molecular mechanisms that determine FDG uptake - a tool that can monitor tumor heterogeneity - remain poorly understood. In this study, we compared FDG uptake in mammary tumors driven by the Akt1, c-MYC, HER2/neu, Wnt1 or H-Ras oncogenes in genetically engineered mice, correlating it to tumor growth, cell proliferation and levels of gene expression involved in key steps of glycolytic metabolism. We found that FDG uptake by tumors was dictated principally by the driver oncogene and was not independently associated with tumor growth or cellular proliferation. Oncogene downregulation resulted in a rapid decrease in FDG uptake, preceding effects on tumor regression, irrespective of the baseline level of uptake. FDG uptake correlated positively with expression of hexokinase-2 (HK2) and HIF-1α and associated negatively with PFK-2b expression and p-AMPK. The correlation of HK2 and FDG uptake was independent of all variables tested, including the initiating oncogene, suggesting that HK2 is an independent predictor of FDG uptake. In contrast, expression of Glut1 was correlated with FDG uptake only in tumors driven by Akt or HER2/neu. Together, these results showed that the oncogenic pathway activated within a tumor is a primary determinant of its FDG uptake, mediated by key glycolytic enzymes that provide a framework to interpret effects on this key parameter in clinical imaging.

*To whom correspondence should be addressed: Lewis A. Chodosh, M.D., Ph.D., chodosh@mail.med.upenn.edu, Room 612 BRB II/III, 421 Curie Boulevard, Philadelphia, PA 19104-6160, USA .

The authors declare that they have no conflicts of interest relevant to this work.

Keywords

fluorodeoxyglucose; positron emission tomography; glycolysis; breast cancer; mouse models

Introduction

The Warburg Effect describes the phenomenon whereby tumor cells preferentially use glycolysis for ATP generation even in the presence of oxygen (1). This increase in glucose utilization by tumor cells enables the imaging of tumors by positron emission tomography (PET) using the tracer F-18-2-fluoro-2-deoxyglucose (FDG). Measurement of FDG uptake in human cancers has broad clinical utility, aiding in the detection, staging and prognosis of tumors, as well as in monitoring their response to therapy. In breast cancer patients, FDG-PET can be used to detect axillary nodal metastasis, locoregional recurrences and distant metastasis (2), and high levels of FDG uptake are associated with a poor prognosis (3-5). Furthermore, a decrease in FDG levels in response to therapy is a useful predictor of a tumor's ultimate response to treatment (6-9). Thus, FDG levels carry important clinical information regarding tumor progression and response to therapy.

In contrast to the well-documented clinical utility of FDG-PET imaging, the cellular and molecular mechanisms that determine FDG-PET uptake in breast cancers – and that underlie the substantial heterogeneity in FDG uptake observed among breast cancers – are poorly understood. Initial studies focused on the idea that high FDG uptake correlates with clinically "aggressive" tumors, in which high uptake was simply thought to reflect the greater metabolic demand of such tumors. Indeed, some studies have shown a trend toward higher FDG uptake in poorly differentiated tumors (10,11), high-grade tumors (12), and tumors with high proliferation rates (10,13). However, the observed correlation between FDG uptake and these histopathologic parameters is, at best, modest (10-13). Furthermore, these general associations fail to explain the mechanisms that might underlie an association between elevated FDG uptake and aggressive tumors.

More recent studies have focused on the molecular mechanisms by which FDG accumulates in tumor cells. Both glucose and FDG are transported into cells via facilitative transport through the GLUT family of cell surface transporters. There are 14 GLUT genes in humans, 11 of which encode proteins possessing glucose transport activity (14). Glucose can also be actively transported into cells by the sodium-dependent transporter SGLT1, though FDG has been reported to be a poor substrate for SGLT1 (15). Once in the cell, glucose and FDG are phosphorylated by hexokinase-1 (HK1) or hexokinase-2 (HK2) and trapped within the cell. While glucose-6-phosphate can enter into the glycolytic pathway, FDG-6-phosphate cannot and therefore accumulates in the cell.

In light of the above, an association would be anticipated to exist between FDG uptake in cancers and the expression levels and activity of both glucose transporters and hexokinases. Indeed, some studies have observed a correlation between Glut1 expression and FDG uptake in human breast cancers (13,16), however others have not (10). Similarly, HK1 expression was significantly associated with FDG uptake in breast cancers in one study (13), whereas two studies did not observe a relationship between FDG uptake and HK2 expression (13,16).

While the basis for this discrepancy is unknown, it is possible that molecular heterogeneity among human breast cancers may confound these analyses, which would suggest the utility of examining correlates of FDG uptake in genetically-defined systems.

Like breast cancer, studies of other tumor types have also failed to reach a consensus on the relationship between FDG uptake and the expression of Glut1, HK1, and HK2. For instance, Glut1 expression has been associated with FDG uptake in some (17-19), but not all (20), human lung cancers. Associations between Glut1 levels and FDG uptake have also been observed in ovarian cancers, pancreatic cancers, colon cancers, gliomas and cholangiocellular carcinomas (19,21-24), but not in esophageal cancers (25). HK2 expression was correlated with FDG levels in esophageal and cholangiocarcinomas (18,24,25), but not in oral squamous cell carcinomas (17,26), and conflicting observations have been reported for this association in lung cancers (17,18,24-26). Thus, while the combined expression of Glut1, HK1 and HK2 likely play some role in determining FDG uptake, the presence and strength of these associations appear to vary among tumor types, and conclusive evidence for one protein playing a dominant role in regulating FDG uptake is lacking.

Recent work suggests that an important function of oncogene activation is the regulation of metabolic pathways that enable cancer cell growth and proliferation. Beyond regulating the expression and activity of genes involved in cell proliferation, growth and survival, oncogene activation also alters metabolic enzymes to support the energetic and biosynthetic demands of anabolic growth (27-30). Indeed, a number of oncogenes impinge directly on enzymes in the glycolytic pathway, and so may account for the altered glucose metabolism observed in tumors. For example, the PI3K-Akt pathway regulates cellular metabolism at multiple nodes, promoting glucose transport, increasing the rate of glycolysis, and stimulating lipid synthesis (reviewed in (28)). These effects are at due, in part, to Akt's ability to promote Glut1 membrane localization and HK2 activation (31). Similarly, c-myc regulates the transcription of genes involved in nearly every step of the glycolytic pathway, including HK2, and enhances aerobic glycolysis (1,32). Moreover, oncogenic Ras activation increases the rate of glycolysis, though the precise mechanism remains unclear (27,33,34). As such, it is apparent that oncogene activation contributes to increased glucose metabolism in cancer cells, however the mechanisms by which this is achieved in different cancers may vary.

Breast cancers exhibit significant histological and molecular heterogeneity, which is likely related to differences in the spectrum of oncogenic pathways driving their malignant growth (35). In light of this, we considered the possibility that FDG uptake in a given tumor might be directly controlled by the specific oncogenic pathways activated within that tumor. The corollary to this proposition is that the heterogeneity of FDG uptake observed across different cancers reflects the heterogeneous molecular alterations present in these cancers. Consistent with this hypothesis, invasive lobular carcinomas (ILCs), which are thought to contain distinct molecular abnormalities from invasive ductal carcinomas (IDCs), exhibit relatively low FDG uptake compared to IDCs (36,37). Furthermore, triple-negative breast cancers that lack expression of HER2, estrogen receptor (ER) and progesterone receptor

(PR) (ER-/PR-/HER2-) exhibit significantly higher uptake than ER+/PR+/HER2− tumors (38,39).

To address the relationship between oncogenic pathway activation and FDG-PET uptake, we evaluated FDG uptake in a set of related inducible transgenic mouse models of breast cancer driven by five distinct oncogenes relevant to human breast cancer. Our data demonstrate that distinct oncogenic pathways differentially regulate glycolytic enzymes and suggest that this differential regulation specifies FDG uptake and underlies at least some of the heterogeneity in FDG uptake observed across cancers.

Materials and Methods

Transgenic mouse lines

MMTV-rtTA mice (*MTB*) expressing the reverse tetracycline transactivator (rtTA) in mammary epithelial cells have been described (40). Responder mice, in which an oncogene is placed under control of the tetracycline promoter (TetOp-Oncogene, or Tet-Onc mice), included constitutively active Akt1 (myristoylated Akt1; *tAKT1*), MYC (*TOM*), Wnt1 (*TWNT*), activated HER2/neu (NeuNT; *TAN*), or mutant H-Ras (*TRAS*). *MTB* mice were crossed with Tet-Onc mice to produce bitransgenic mice in which oncogene expression could be inducibly expressed in the mammary gland by addition of doxycycline to the drinking water. *MTB/tAKT1*, *MTB/TOM*, *MTB/TWNT*, *MTB/TAN*, and *MTB/TRAS* bitransgenic mice have been described (41-45). A second line permitting inducible expression of myristoylated Akt1 in the mammary gland, termed TMILA-AKT1 (*TAKT1*), was also generated (data not shown). Both tAKT1 and TMILA-AKT1 mice express active, myristoylated Akt1 in a mammary epithelial-specific manner. TMILA-AKT1 also expresses a luciferase reporter gene downstream from an IRES sequence, allowing for in vivo imaging of tumor cells. The two models exhibit similar tumor latencies, tumor growth, and FDG uptake; given their similar behavior, *MTB/tAKT1* and *MTB/TAKT1* mice were considered as one group.

Bitransgenic mice were administered doxycycline (dox) in their drinking water beginning at 6 weeks of age. The dose of doxycycline was 2 mg/ml with 5% sucrose for *MTB/TAKT1*, *MTB/TOM* and *MTB/TWNT* mice, 0.1 mg/mL for *MTB/tAKT1* and *MTB/TAN* mice, and 0.012 mg/mL for *MTB/TRAS* mice. Doxycycline bottles were changed once per week. Mice were monitored twice per week for tumor formation. The latency of tumor formation after initiation of doxycycline treatment was 15 weeks in *MTB/AKT* mice, 22 weeks in *MTB/TOM* mice, 20 weeks in *MTB/TWNT* mice, 12 weeks in *MTB/TAN* mice, and 11 weeks in *MTB/TRAS* mice. Tumors in these models arise in all 10 mammary glands, though tumors are somewhat more common in glands #1 and #2. Calipers were used to measure tumor diameter in two dimensions and tumor volume was computed based on an elliptical model: volume=width×width×length×π/6 (46). All animal studies were conducted humanely according to protocols approved by the University of Pennsylvania Institutional Animal Care and Use Committee (IACUC).

PET imaging

PET imaging was performed on a prototype dedicated small-animal PET scanner (A-PET) developed at the University of Pennsylvania (47,48). Technical details of the prototype scanner are similar to the commercial Mosaic HP scanner from Philips Healthcare (Cleveland, OH). PET acquisition parameters have been described (47,48). In brief, the scanner uses 2×2×10 mm lutetium (yttrium) orthosilicate (LYSO) crystals with 2.3-mm pitch, resulting in a transverse spatial resolution of 2.3 mm and axial spatial resolution of 2.4 mm. The detector diameter is 19.7 cm with an axial length of 11.6 cm. The system is fully 3D without inter-plane septa to maximize sensitivity, and utilizes the 3D row-action maximum likelihood algorithm (3D RAMLA) for image reconstruction (49). Data were reconstructed into images with 0.5 mm^3 voxels, resulting in 240 parallel transverse slices. Random subtraction and decay correction were applied to the data. Scatter and attenuation correction were not applied.

Mice were scanned once tumor sizes reached approximately 1 cm in diameter. Preference was given to imaging mice bearing tumors in the #3 glands to avoid background from neighboring normal anatomical structures with high FDG uptake. Mice were fasted at least 3 hours prior to PET scanning, during which time the drinking water for *MTB/TAKT1*, *MTB/TOM*, and *MTB/TWNT* mice was switched to 0.5 mg/mL doxycycline without sucrose to reduce potential effects of ingested glucose on FDG uptake. Mice received 0.4 – 0.6 mCi of [^{18}F]-FDG via tail vein injection. PET scanning was performed 2 hr post-injection. Mice were anesthetized with 1-2% isoflurane via inhalation delivered in oxygen at a flow rate of 1.0 L/min through a nose cone immediately prior to and during scan.

PET image analysis

PET image analysis was performed using Amide (A Medical Image Data Examiner) software. The average background uptake for the mouse, excluding regions of high uptake (the bladder, heart, tail, and tumor) was calculated as: Uptake(background) = counts(whole mouse) – counts(bladder) – counts(heart) – counts(tail) – counts(tumor)/pixels(whole mouse) – pixels(bladder) – pixels(heart) – pixels(tail) – pixels(tumor). A semi-automated region of interest (ROI) was generated surrounding each tumor in three dimensions by drawing an isocontour with a threshold equal to the calculated average background uptake of the mouse. Adjustments to the ROI were made manually to exclude adjacent non-tumor structures with isointense FDG uptake.

Two approaches were used to measure FDG uptake within this ROI. First, the mean FDG uptake was calculated as: Mean Uptake(tumor) = counts(tumor)/pixels(tumor). Alternatively, the maximum FDG uptake within the tumor was calculated as: Max uptake(tumor) = $counts_{>0.9max}$(tumor)/pixels(tumor). The mean or max uptake for each tumor was then normalized to the background uptake as: Normalized Uptake(tumor) = Uptake(tumor)/Uptake(background). The FDG uptake index is therefore a unitless value where an uptake index (UI) > 1 corresponds to FDG uptake above background. The average normalized mean or max FDG uptake and the standard error of the mean were calculated for tumors arising in each bitransgenic mouse line.

QRT-PCR, immunoblotting, and immunofluorescence analysis of glycolytic genes

For analysis of gene expression, tumor-bearing mice were sacrificed following PET scanning. Tumor tissue was then harvested and either frozen in optimal cutting temperature compound (OCT) for immunofluorescence (IF) or snap frozen for biochemical analysis. IF analysis of Glut1 was performed as described (41). For determination of tumor proliferation rates, sections were stained with antibodies against Ki67 (1:50; Ki-S5, Dako, Carpinteria, CA) and cytokeratin 8 (CK8, 1:50; TROMA-1, Developmental Studies Hybridoma Bank, Iowa City, IA). Sections were counterstained with Hoechst 33258 (Sigma, St Louis, MO) prior to imaging. Images from stained sections were captured digitally and areas of positively stained and unstained nuclei were quantified by color segmentation analysis using Image-Pro Plus software (Media Cybernetics, Silver Spring, Maryland). Quantitative analysis was performed on 4 fields per section consisting of approximately 2,500–10,000 cells. The percentage of Ki67-positive cells was computed by dividing total Ki67-positive cells by total CK8-positive cells.

For detection of transcript levels, RNA was extracted and reverse transcribed, and quantitative RT-PCR was performed as described (45). Briefly, 2 ug RNA was reverse transcribed to cDNA using the High Capacity cDNA Reverse Transcription Kit (Applied Biosystems, Foster City, CA) according to the manufacturer's instructions. Expression levels of glycolytic genes were assessed by real-time quantitative PCR (Q-PCR) on a 7900HT instrument (Applied Biosystems) using the following TaqMan assays: Hexokinase-1 (Mm00439344_m1), Hexokinase-2 (Mm00443385_m1), Slc2a1 (Mm00441473_m1), Slc2a4 (Mm01245507_g1), Slc2a6 (Mm00554217_m1), Slc2a8 (Mm00444634_m1), Slc2a9 (Mm01211147_m1), Slc2a10 (Mm00453716_m1), Slc2a12 (Mm00619244_m1), Slc5a1 (Mm00451203_m1), Pfkb1 (Mm01260986_m1), Pfkb2 (Mm00435575_m1), Pfkp (Mm00444792_m1), and Tbp (Mm00446973_m1). Expression levels were normalized to Tbp.

Immunoblotting analysis was performed as described (41), with the exception of Glut1 western blotting, which was performed using a modified protocol to minimize Glut1 aggregation (50). Antibodies used were: Glut1 (1:5000, kindly provided by Dr. Morris Birnbaum, University of Pennsylvania), Hexokinase-2 (C4G5, 1:1000, Cell Signaling, Beverly, MA) Glut4 (1:1000, Cell Signaling), p-mTOR (p-S2448, 1:1000, Cell Signaling), p-AMPK (p-T172, 1:1000, Cell Signaling), p-S6 (p-S235/236, 1:1000, Cell Signaling), and p-PFK2 (p-S483, 1:1000, Santa Cruz Biotechnology, Santa Cruz, CA). Primary antibodies were detected with appropriate secondary antibodies conjugated to infrared dyes (Alexa 680, Molecular Probes or IRDye 800CW, LI-COR) using an Odyssey Infrared Imaging System (LI-COR Biosciences, Lincoln, NE). Levels of Glut1, Glut4, HK2, p-PFK2, and p-AMPK were normalized to tubulin, and p-S6 and p-mTOR were normalized to levels of total S6 and total mTOR, respectively.

Statistical methods

ANOVA was used to compare global variations in FDG uptake across tumors arising in different lines, and two-tailed t-tests were used to compare differences in FDG uptake between pairs of lines. A linear regression test was used to evaluate correlations between

FDG uptake and gene expression, protein expression, protein phosphorylation, and proliferation. A *p* value of less than 0.05 was considered significant, while values between 0.05 and 0.1 were considered marginally significant. F-tests were used to assess the significance of regression model improvement after adding an additional explanatory variable.

To identify a regression model that incorporated predictive abilities of more than two variables, we used the "exhaustive search" approach (51) on all possible 3- to 9-variable linear regression models. Each variable was evaluated in models either untransformed or log-transformed, depending on which version provided lower leave-one-out cross validation error in a single-variable model. Four types of model-selection criteria (adjusted R^2, PRESS, AIC and SBC) were employed to identify top performing multivariate models, from which one final model was selected that had the best balance between predictive power and model complexity.

Results

FDG uptake in mouse mammary tumors is determined by the initiating oncogene

To better understand the molecular and cellular basis for variation in FDG uptake observed across different human breast cancers, as well as its potential association with specific oncogenic alterations, we evaluated FDG uptake in five related, genetically-defined mouse models of breast cancer. We have previously described the generation and characterization of inducible bitransgenic mice in which MYC (*MTB/TOM*), activated HER2/neu (*MTB/TAN*), Wnt1 (*MTB/TWNT*), myristoylated Akt1 (*MTB/TAKT*), or mutant v-Ha-Ras (*MTB/TRAS*) can be conditionally expressed in the mammary gland in a doxycycline-dependent manner (41-44,52). Expression of each oncogene induced by doxycycline administration in the drinking water results in the formation of mammary adenocarcinomas with high penetrance and latencies ranging from 11 to 22 weeks. Tumors arising in each model exhibit distinct morphologies, though they each exhibit an epithelial morphology and recapitulate the diverse morphologies of human ductal carcinomas. In addition, activation of each of the oncogenes gives rise to tumors that are invasive and metastasize to distant sites.

Doxycycline was administered to Akt, MYC, Wnt1, HER2/neu, and Ras mice beginning at 6 weeks of age and mice were monitored for tumor formation. Following its initial detection, each tumor was palpated twice weekly to monitor tumor growth. Tumors from each model exhibited similar growth rates.

To compare glucose uptake in tumors driven by each oncogene, FDG-PET was performed once tumors reached approximately 1 cm in diameter. Tumors driven by each oncogene exhibited elevated FDG uptake compared to the background level of uptake observed in normal tissue (Figure 1A). To obtain a quantitative assessment of FDG uptake, PET imaging was performed on a large cohort of Akt (n=14), MYC (n=19), Wnt1 (n=16), HER2/neu (n=21), and Ras (n=12) tumors and FDG uptake was measured by calculating an uptake index (UI) as described in Methods. Both mean and max uptake were calculated, as both values have been used in clinical settings.

Quantitative analysis revealed that Akt-driven tumors exhibited the highest FDG uptake, followed in descending order by MYC-, Wnt1-, HER2/neu- and Ras-driven tumors. Indeed, both mean and max levels of FDG uptake differed significantly between tumors of different genotypes (Figure 1B and C), and the variation in FDG uptake between tumors of different genotypes was greater than the variation in FDG uptake within tumors of a given genotype ($p<0.0001$, overall ANOVA). Overall, Akt- and MYC-driven mammary tumors exhibited significantly higher FDG uptakes than Wnt1-, HER2/neu-, or Ras-driven tumors (Figure 1B and C). Results were similar whether evaluating the mean or max uptake index. Since the correlation between these values was high ($r=0.91$), only the mean uptake was used for subsequent analyses. These results suggest that tumor FDG uptake is significantly influenced by the particular oncogene driving tumor growth and development.

FDG uptake decreases following acute oncogene down-regulation

Decreases in FDG uptake may be an early predictor of responses to antineoplastic therapy (53). Given that oncogene down-regulation in inducible models can be viewed as a genetic surrogate for targeted therapy, we asked whether we could detect changes in FDG uptake shortly after oncogene down-regulation, at time-points preceding detectable tumor regression. Doxycycline was withdrawn from mice bearing 1 cm tumors to initiate oncogene down-regulation, and FDG was measured serially at 0, 2 and 4 days following doxycycline removal. Oncogene down-regulation led to a marked and rapid reduction in FDG uptake in tumors from each genotype, irrespective of the oncogenic pathway driving the tumor or the baseline level of FDG uptake (Figure 1D). Notably, the reduction in FDG uptake in Ras tumors was variable. At 4 days following Ras de-induction, FDG uptake had decreased by 40-50% in 3 tumors and by 20-30% in an additional 3 tumors (Supplemental Figure 1). In contrast, FDG uptake showed no decrease or a modest increase in 2 tumors (Supplemental Figure 1). In aggregate, these findings confirm that elevated FDG uptake in tumors is a consequence of oncogene activation and, furthermore, is consistent with observations in cancer patients that treatment with targeted therapies can result in decreased FDG uptake (29).

Proliferation is not an independent predictor of FDG uptake

While a number of studies have found that FDG uptake is higher in rapidly proliferating tumors, the mechanism underlying this relationship is unclear. Ostensibly, pathways that drive proliferation could indirectly stimulate glucose uptake as a secondary consequence of the metabolic demands of proliferation. Alternately, glucose uptake could be rate-limiting for proliferation, such that tumors with high proliferation rates are by definition tumors that are able to avidly transport and trap glucose. A third possibility is that the same molecular pathways that drive cell proliferation may directly promote glucose uptake in parallel, in which case uptake and proliferation would be correlated but mechanistically unrelated.

To distinguish between these possibilities we examined the relationship between FDG uptake, tumor growth and tumor cell proliferation, as well as whether this relationship was independent of the oncogene driving tumor growth. Growth rates of mammary tumors did not vary significantly by oncogenic pathway. Indeed, tumors induced by MYC and Akt,

which exhibited the highest FDG uptake, had – if anything – the lowest growth rates (Figure 2A). This suggests that FDG uptake is not merely a consequence of rapid tumor growth.

We next assessed rates of cellular proliferation by measuring the fraction of mammary tumor cells expressing the proliferation antigen Ki67 (Figure 2B). MYC-driven tumors had a significantly higher fraction of Ki67-positive cells than tumors induced by other oncogenes. In contrast, Akt-driven tumors had relatively low proliferation rates, despite the fact that they exhibited high FDG uptakes comparable to tumors induced by MYC. This suggests that FDG uptake is not simply a consequence of rapidly proliferating tumor cells.

We next examined the correlation between proliferation rate and FDG uptake across 30 individual tumors. We observed a modest but significant association, with highly proliferative tumors generally exhibiting higher FDG uptake (Figure 2C; r^2=0.16, p=.029). These results are consistent with findings in human tumors, and suggest that some correlation exists between FDG uptake and cellular proliferation.

However, closer examination of the relationship between tumor cell proliferation and FDG uptake revealed that the observed correlation was principally due to the fact that MYC-induced tumors exhibit both high FDG uptake and rapid proliferation. Consistent with this, removing MYC tumors from the analysis abrogated the apparent relationship between FDG uptake and proliferation (r^2=0.0006, p=0.92).

Similarly, no correlation was observed between cellular proliferation rates and FDG uptake within tumors of any given genotype (Figure 2D). Indeed, on multivariate analysis the relationship between proliferation and uptake was lost after adjusting for tumor genotype (Supplemental Table 1, p=0.71). These findings indicate that the oncogenic pathway activated within a tumor is a more important determinant of FDG uptake than the proliferative rate of that tumor, and further suggest that the reported relationship between FDG uptake and proliferation in human breast cancers may be an indirect consequence of an association between cellular proliferation rates and the activation of specific oncogenic pathways.

Expression of HK2, but not HK1 or Glut1, is correlated with FDG uptake

In light of conflicting clinical studies on the association between FDG uptake and expression of HK1, HK2 and Glut1, we examined the relationship between these parameters in mouse mammary tumors driven by each of the five oncogenic pathways evaluated in this study. HK1, HK2 and Glut1 expression were analyzed at both the mRNA and protein level using qRT-PCR and quantitative western blotting in 6 tumors for each oncogene. Glut1 membrane localization was also assessed using immunofluorescence, since the membrane localization of this transporter is regulated by Akt (31). Glut1 was localized to the cell membrane in all tumors examined (data not shown), therefore total Glut1 protein was used as a proxy for membrane-localized Glut1.

We calculated the Pearson correlation coefficient between each gene and FDG uptake across all tumors examined. High HK2 protein levels were strongly correlated with high uptake across all tumors (Figure 3A; r^2=0.339, p=0.001). Levels of Glut1 protein and HK2 mRNA

exhibited a modest association with FDG uptake, though this did not reach statistical significance (Figure 3B and 3D; Glut1 protein: r^2=0.078, p=0.136; HK2 mRNA: r2=0.073, p=0.149). In contrast, levels of HK1 protein (Figure 3C), and the levels of Glut1and HK2 mRNA (Figure 3E and F) were not correlated with FDG uptake.

These results demonstrate that FDG uptake is strongly associated with HK2 protein levels in genetically defined mouse mammary tumors, and suggest that HK2 expression may represent an important determinant of glucose uptake in mammary tumor cells.

Quantitative assessment of glycolytic and energy-sensing pathways

The above results suggested that FDG uptake in genetically defined mouse mammary tumors might be determined by oncogene-induced and oncogene-specific changes in expression of Glut1, HK1, and HK2. However, while we observed significant correlations between HK2 and FDG uptake in mammary tumors induced by different oncogenic pathways, the modest strength of these associations suggested that other factors might contribute to the determination of FDG uptake. Therefore, we analyzed the expression of other genes involved in glucose transport and metabolism.

We focused on proteins that mediate three critical steps of glycolysis: transport of glucose into the cell by Glut or SGLT family transporters; phosphorylation of glucose by hexokinases to generate glucose-6-phosphate; and phosphorylation of fructose-6-phosphate by phosphofructokinase to generate fructose-1,6-bisphosphate (Figure 4A). In addition, we evaluated the AMPK-mTOR pathway since we reasoned that examination of pathways responsible for energy sensing in cells could provide insight into the bioenergetic consequences of glucose uptake in tumors (Figure 4A). Finally, we examined expression of HIF-1α in light of the well-established role of HIF-1α in regulating glycolysis.

We measured the expression of each of the above genes and proteins involved in glucose transport, phosphofructokinase activity, AMPK-mTOR pathway activity, and HIF-1α pathway activity (shown in red in Figure 4A) in a cohort of 30 tumors arising in *MTB/TAKT*, *MTB/TWNT*, *MTB/TOM*, *MTB/TAN* and *MTB/TRAS* mice (six tumors per genotype) (Figure 4B).

Unsupervised hierarchical clustering of tumors based on the expression of this set of genes and proteins largely grouped tumors by the initiating oncogene (Figure 4B). Akt-driven tumors were characterized by high expression of a cluster of genes including Glut1, p-mTOR and several other Slc family glucose transporters. MYC-driven tumors were characterized by high expression of HK2 and HIF-1α, and HER2/neu- and Ras-driven tumors expressed high levels of HK1, PFK-1 and p-AMPK (Figure 4B). These results confirm that tumors of different genotypes exhibit unique patterns of glycolytic gene expression.

To examine the molecular correlates of FDG uptake in this cohort of tumors, we calculated the Pearson correlation coefficient between each gene or protein and FDG uptake in HER2/neu, MYC, Akt, Wnt1, and Ras-induced tumors (Table 1). None of the other glucose transporters examined was positively correlated with FDG uptake across all tumors.

However, FDG uptake was strongly correlated with expression of Glut12 in Ras-driven tumors (r=0.847, p=0.034), raising the possibility that this transporter may specifically play a role in tumors driven by this oncogene.

Expression levels of PFK-2 mRNA (r= −0.369, p=0.045) and phospho-PFK-2 (r= −0.363, p=0.049) were negatively correlated with FDG uptake (Figure 5A and B). Similarly, an inverse correlation was observed between FDG uptake and AMPK phosphorylation (r= −0.355, p=0.053; Figure 5C). This is consistent with a model in which tumors utilizing high levels of glucose have a high ATP:AMP ratio and, consequently, suppress the AMPK pathway. No association was observed between FDG uptake and activation of mTOR or S6, consistent with the notion that these proteins can be regulated by a variety of upstream pathways other than the AMPK energy-sensing pathway. Consistent with this, we did not observe any correlation between AMPK activation and mTOR or S6 activation (data not shown).

Finally, levels of HIF-1α were marginally correlated with FDG uptake although this did not reach statistical significance (r=0.344, p=0.063; Figure 5D). This was largely attributable to the fact that MYC tumors exhibited high levels of HIF-1α as well as high levels of FDG uptake. This finding is consistent with previous reports on the relationship between MYC and HIF in regulating tumor cell metabolism.

In aggregate, these data indicate that high FDG uptake is associated with elevated expression of HK2 and HIF-1α, as well as suppression of PFK-2 and AMPK activity. This, in turn, suggests that FDG uptake is correlated with critical steps of glucose metabolism, including phosphorylation to generate glucose-6-phosphate and fructose-2,6-bisphosphate, and provide in vivo confirmation that FDG uptake is associated with the energy status of tumor cells.

HK2 is independently associated with FDG uptake

Our results to this point indicated that expression of HK2 and HIF-1α are positively associated with FDG uptake, whereas the activity of PFK-2 and AMPK are negatively associated with uptake. Our data further showed that the identity of the oncogenic pathway driving tumor growth is a major determinant of FDG uptake, and that FDG uptake is modestly associated with of tumor proliferation rates. We next examined which of these determinants of FDG uptake is independently associated with uptake. To accomplish this, we individually adjusted for each of these variables and then asked whether inclusion of a second variable significantly improved the observed correlation with FDG uptake.

After adjusting for genotype, only HK2 retained its association with FDG uptake, indicating that the association between FDG uptake and HK2 expression is independent of the oncogenic pathway activated in the tumor (Supplemental Table 1).

We next asked whether the differences in FDG uptake observed across tumors induced by different oncogenes could be explained by variation in the expression of these glycolytic and energy sensing genes. To address this, we determined whether tumor genotype remained associated with FDG uptake after adjusting for the expression of HK2, Glut1, p-Pfk2, p-

Ampk, or HIF-1α This revealed that the association between tumor genotype and FDG uptake was lost after adjusting for HK2 (Supplemental Table 1). In contrast, the association between tumor genotype and FDG uptake remained significant after individually adjusting for Glut1, p-Pfk2, and p-Ampk, and remained marginally significant after adjusting for HIF-1α and cellular proliferation. These findings indicate that a substantial fraction of the variation in uptake observed between tumors driven by different oncogenes can be explained by differences in HK2 expression. HK2 expression may also be responsible for differences in FDG uptake within tumors driven by the same oncogene, though additional tumors would be needed to provide sufficient statistical power to detect this association.

Finally, we examined whether HK2, Glut1, p-Pfk2, p-Ampk, HIF-1α and cellular proliferation were associated with FDG uptake independently of each other. We found that HK2 was correlated with uptake after correcting for every other individual variable tested, indicating that HK2 expression is a strong and independent predictor of FDG uptake (Supplemental Table 1). Conversely, only p-Ampk remained significantly associated with uptake after adjusting for HK2 expression, suggesting that p-Ampk and HK2 are associated with FDG uptake independently of one another.

In sum, these findings indicate that HK2 is associated with FDG uptake independently of each of the variables evaluated in this study, including the oncogenic pathway activated with the tumor as well as its proliferative rate.

Multivariate analysis of FDG uptake

Our findings revealed that expression of HK2 accounted for 34.2% of the observed variation in FDG uptake (Figure 3 and Table 1; r^2=0.342, p=0.001) and that, among all variables tested, only p-Ampk was associated with FDG uptake independently of HK2. Together, HK2 and p-Ampk accounted for 44.1% of the observed variation in uptake (Supplemental Table 1).

We next attempted to construct a model with improved predictive power by including additional variables. To achieve this, we used the “exhaustive search” approach (51) to examine all possible models with 3 to 9 variables using four different model-selection criteria. We found a 6-variable model that could account for 77.9% of the observed variation in FDG uptake (Supplemental Table 2, Supplemental Figure 2). This model included variables that are positively correlated with uptake (HK2 and Glut1), as well as variables negatively correlated with uptake (p-AMPK, p-PFK2, SGLT1, and proliferation rate). This analysis indicates that expression levels of these six glycolytic and energy-sensing genes can explain the majority of variation in glucose uptake observed across mammary tumors induced by the HER2/neu, MYC, Wnt1, Akt and Ras oncogenes.

Oncogene-specific correlates of FDG uptake

Different oncogenes impinge on the glycolytic pathway at different nodes. As such, FDG uptake may be determined by different mechanisms in tumors in which different oncogenic pathways have been activated. We therefore asked how the expression of HK1, HK2, and Glut1 varied among tumors driven by different oncogenes, and whether the relationship

between FDG uptake and expression of HK1, HK2, and Glut1 was dependent upon the oncogene driving tumorigenesis.

Both HK1 mRNA (Figure 6A) and protein (data not shown) were expressed at significantly higher levels in Ras-driven tumors compared to tumors driven by other oncogenes ($p<0.0001$, ANOVA). In contrast, HK2 protein expression was substantially higher in Myc-driven tumors than tumors of other genotypes (Figure 6B; $p<0.0001$, ANOVA) and Glut1 protein expression was modestly higher in Akt-driven tumors than tumors of other genotypes, though this did not reach statistical significance (Figure 6C; $p=0.055$, ANOVA). Consequently, when compared to tumors induced by other oncogenes, MYC-driven tumors had higher levels of HK2 expression and lower levels of Glut1, suggesting that glucose phosphorylation by HK2 may be a more critical determinant of uptake than glucose transport by Glut1 in these tumors. In contrast, Akt tumors had higher levels of Glut1 and relatively low levels of HK2, suggesting that Glut1 may be a more important determinant of FDG uptake in Akt-driven tumors. This suggests that different oncogenes differentially regulate core glycolytic genes.

We next calculated the Pearson correlation coefficient between each of these variables and FDG uptake for 6 tumors of each genotype. Notably, these results suggested that FDG uptake may exhibit different associations with HK1, HK2 and Glut1 in tumors driven by different oncogenes. For instance, Glut1 levels were strongly correlated with FDG uptake in Akt- and HER2/neu-driven tumors, whereas no association was found between Glut1 levels and FDG uptake in MYC-, Wnt1-, or Ras-driven tumors (Figure 6D). This suggests that the borderline association observed between FDG uptake and Glut1 protein levels across all tumors ($r^2=0.078$, $p=0.136$) is, in fact, the result of combining a strong association between these parameters in tumors induced by the Akt and HER2/neu pathways (e.g., Akt, $r^2=0.846$, $p=0.009$; HER2/neu, $r^2=0.882$, $p=0.005$) with the lack of such an association in tumors induced by the other three oncogenic pathways examined.

As further evidence of the potential existence of oncogene-specific metabolic associations, when considering tumors induced by each of the five oncogenic pathways studied, only Ras-driven tumors exhibited a trend towards a correlation between *HK1* mRNA expression and FDG uptake (Figure 6F; $r^2=0.489$, $p=0.12$). While this did not reach statistical significance, likely due to the small number of tumors examined (n=6), when combined with the observation that Ras-driven tumors express high levels of HK1, this raises the possibility that Ras-driven tumors may utilize HK1, rather than HK2, to phosphorylate and trap FDG.

In aggregate, our results suggest that FDG uptake in tumors induced by different oncogenic pathways may be determined by mechanisms involving changes in the expression of different glycolytic enzymes.

Discussion

Measurement of FDG-PET uptake provides clinically useful information regarding human cancers, including information about prognosis and response to therapy. However since the determinants of FDG uptake in tumors have yet to be fully elucidated, the biological

meaning – and therefore appropriate clinical interpretation – of a PET scan showing a high level of FDG uptake in a human cancer is incompletely understood. Most studies to date attempting to address this issue have examined the relationship between FDG uptake and molecular or cellular features of human cancers. Unfortunately, the power of this approach is limited by the extensive genetic heterogeneity of human tumors, a fact that may have contributed to the limited success of these approaches in identifying consistent correlates of FDG uptake.

We reasoned that genetically engineered mouse models would provide an alternate means to investigate the molecular and cellular determinants of FDG uptake in tumors. Because tumors arising in these mice have genetically defined initiating events and arise in genetically identical hosts, we anticipated that they would provide a more powerful approach to identifying molecular correlates of FDG uptake, particularly with respect to the relationship between FDG uptake and the activation of oncogenic pathways relevant to human cancer.

Human breast cancers comprise a spectrum of histological subtypes whose differing biological properties are thought to be driven by the different spectrum of molecular alterations present in each subtype. In this regard, our studies of mammary tumors induced by five different oncogenes relevant to human cancer revealed that the oncogenic pathway driving tumor growth and development is a principal determinant of FDG uptake. Specifically, tumors initiated and driven by Akt or MYC exhibited the highest levels of FDG uptake, with lower levels of FDG uptake observed for Wnt1, HER2/neu and Ras-driven tumors, despite the fact that tumors induced by each of these oncogenic pathways grew at comparable rates in vivo. As such, our findings suggest that the heterogeneity in FDG uptake observed among human breast cancers may be a consequence of the different oncogenic pathways activated within these tumors.

In the clinical literature, FDG-PET uptake has frequently been taken as a surrogate marker for aggressive or rapid tumor growth. In contrast to this assumption, we observed marked differences in FDG uptake across tumors induced by the Akt, MYC, HER2/neu, Wnt1 and Ras oncogenes, despite similar rates of growth for tumors driven by these different pathways. Moreover, while FDG uptake has repeatedly been shown to correlate with tumor cell proliferation, we found that the modest association between FDG uptake and cellular proliferation rate was largely attributable to the fact that MYC-induced tumors exhibited both high FDG uptake and rapid proliferation. Indeed, no association between cellular proliferation and uptake was observed among the 24 tumors induced by the Akt, HER2/neu, Wnt1 and Ras oncogenes. Consistent with this, adjusting for tumor genotype abrogated the relationship between cellular proliferation and FDG uptake. This lack of a direct relationship between FDG uptake and proliferation was highlighted by the observation that while Akt and MYC-induced mammary tumors each exhibited high levels of FDG uptake, MYC-induced tumors had the highest rates of proliferation across all tumors, whereas Akt-induced tumors had amongst the lowest.

The Akt pathway is activated in a significant proportion of human breast cancers, often through mutational activation of its upstream activator PI3K or inactivation of its negative

regulator PTEN. Similarly, *HER2/neu* and *MYC* are each amplified or transcriptionally up-regulated in a substantial fraction of human breast cancers. Our finding that Akt- and Myc-driven mammary tumors exhibit high FDG uptake, whereas HER2/neu-driven mammary tumors exhibit lower FDG uptake, may explain some of the heterogeneity in FDG uptake observed in human breast cancers. Indeed, it is possible that those breast cancers with the highest FDG uptake may harbor constitutive activation of the Akt and/or MYC pathways. This phenomenon may underlie the recently described associations between FDG uptake and breast cancer subtypes (39).

At the molecular level, studies have reported conflicting results regarding the associations between FDG uptake and expression of Glut1, HK1 and HK2. A seminal study by Bos et al. undertook a comprehensive analysis of human breast cancers to identify molecular correlates of FDG uptake (13). They examined a number of markers and found that, in addition to proliferation, expression of Glut1 and HK1 were each significantly associated with FDG uptake whereas expression of HK2 was not. However, an analogous study by Avril et al. failed to find an association between FDG uptake and Glut1 levels (10). Potentially, this discrepancy could be explained by genetic heterogeneity present across human breast cancers and their hosts, since identifying determinants of FDG uptake would be confounded if tumors in which different oncogenic pathways were activated possess different correlates of FDG uptake. This was our rationale for studying FDG uptake in genetically-defined tumors in mice.

Our findings confirm that HK2 protein levels are an independent predictor of FDG uptake across tumors induced by five different oncogenes. However, FDG uptake was strongly correlated with Glut1 expression in Akt- and HER2/neu-driven tumors, whereas no association was found between FDG uptake and Glut1 levels in MYC-, Wnt1-, or Ras-driven tumors. This context-dependence may explain the conflicting findings reported for the relationship between Glut1 levels and FDG uptake in human breast cancers, where some studies have found an association between these parameters (13)while others have not (10). This highlights the fact that bona fide associations between FDG uptake and the expression or activity of specific glycolytic proteins may be obscured by the existence of such associations in breast cancers driven by some, but not other, oncogenic pathways. In an analogous manner, Akt-driven tumors exhibited high levels of Glut1 and relatively low levels of HK2, whereas MYC-driven tumors exhibited high levels of HK2 but low levels of Glut1. This suggests that tumors driven by each of these two oncogenes achieve high FDG uptake through distinct mechanisms.

Interestingly, Ras-driven tumors seem to differ in several respects from tumors driven by other oncogenes. For instance, FDG uptake in Ras-driven tumors was marginally associated with HK1, rather than HK2, expression levels. Furthermore, there was a strong correlation between Glut12 expression and FDG uptake in Ras tumors, but not in tumors driven by other oncogenes. Finally, only a subset of Ras-driven tumors exhibited a decrease in FDG uptake following oncogene down-regulation. In pancreatic cancer, K-Ras is thought to increase glycolysis by up-regulating several glycolytic enzymes, including Glut1, HK1, and HK2 (54). The different behavior of H-Ras-driven tumors in our study may be due to

differences between H-Ras and K-Ras, or between differences between breast and pancreatic cancer cells.

The above observations point to the oncogene-specific regulation of FDG uptake in mammary tumors. As such, an important implication of our findings is that there is no single route to achieving high glucose uptake. This may explain, at least in part, the lack of success in clinical studies in attributing FDG uptake to the expression of any single protein. Rather, our evidence indicates that the oncogenic pathway activated within a tumor largely determines the extent of uptake within that tumor, primarily by regulating the expression and activity of multiple proteins within the glycolytic pathway.

Finally, it is notable that down-regulation of the HER2/neu, MYC, or Wnt1 oncogenes in existing mammary tumors resulted in a rapid and marked reduction in FDG uptake, irrespective of the oncogenic pathway driving the tumor or the baseline level of FDG uptake, and in a manner that preceded regression of the tumor. To the extent that the genetic down-regulation of dominant oncogenic pathways within tumors can be viewed as a genetic surrogate for targeted pharmacological therapies that block these pathways, our findings suggest that decreased FDG uptake may be a common consequence, as well as an early predictor, of response to oncogene inhibition through targeted therapy.

Supplementary Material

Refer to Web version on PubMed Central for supplementary material.

Acknowledgements

We are grateful to Minghua Xu, Paul Acton, Sharon Sudarshan, and Valentina Circiumaru for assistance with FDG-PET scans and Blanche Young and Kathy Notarfrancesco for molecular analyses.

References

1. Kim JW, Dang CV. Cancer’s molecular sweet tooth and the Warburg effect. Cancer research. 2006; 66(18):8927–30. [PubMed: 16982728]
2. Mankoff DA, Eubank WB. Current and future use of positron emission tomography (PET) in breast cancer. Journal of mammary gland biology and neoplasia. 2006; 11(2):125–36. [PubMed: 17075687]
3. Oshida M, Uno K, Suzuki M, Nagashima T, Hashimoto H, Yagata H, et al. Predicting the prognoses of breast carcinoma patients with positron emission tomography using 2-deoxy-2-fluoro[18F]-D-glucose. Cancer. 1998; 82(11):2227–34. [PubMed: 9610703]
4. Mankoff DA, Dunnwald LK, Gralow JR, Ellis GK, Charlop A, Lawton TJ, et al. Blood flow and metabolism in locally advanced breast cancer: relationship to response to therapy. J Nucl Med. 2002; 43(4):500–9. [PubMed: 11937594]
5. Inoue T, Yutani K, Taguchi T, Tamaki Y, Shiba E, Noguchi S. Preoperative evaluation of prognosis in breast cancer patients by [(18)F]2-Deoxy-2-fluoro-D-glucose-positron emission tomography. J Cancer Res Clin Oncol. 2004; 130(5):273–8. [PubMed: 14986112]
6. Wahl RL, Zasadny K, Helvie M, Hutchins GD, Weber B, Cody R. Metabolic monitoring of breast cancer chemohormonotherapy using positron emission tomography: initial evaluation. J Clin Oncol. 1993; 11(11):2101–11. [PubMed: 8229124]
7. Mankoff DA, Dunnwald LK. Changes in Glucose Metabolism and Blood Flow Following Chemotherapy for Breast Cancer. PET Clinics. 2006; 1(1):71–81.

8. Schelling M, Avril N, Nahrig J, Kuhn W, Romer W, Sattler D, et al. Positron emission tomography using [(18)F]Fluorodeoxyglucose for monitoring primary chemotherapy in breast cancer. J Clin Oncol. 2000; 18(8):1689–95. [PubMed: 10764429]

9. Smith IC, Welch AE, Hutcheon AW, Miller ID, Payne S, Chilcott F, et al. Positron emission tomography using [(18)F]-fluorodeoxy-D-glucose to predict the pathologic response of breast cancer to primary chemotherapy. J Clin Oncol. 2000; 18(8):1676–88. [PubMed: 10764428]

10. Avril N, Menzel M, Dose J, Schelling M, Weber W, Janicke F, et al. Glucose metabolism of breast cancer assessed by 18F-FDG PET: histologic and immunohistochemical tissue analysis. J Nucl Med. 2001; 42(1):9–16. [PubMed: 11197987]

11. Adler LP, Crowe JP, al-Kaisi NK, Sunshine JL. Evaluation of breast masses and axillary lymph nodes with [F-18] 2-deoxy-2-fluoro-D-glucose PET. Radiology. 1993; 187(3):743–50. [PubMed: 8497624]

12. Crippa F, Seregni E, Agresti R, Chiesa C, Pascali C, Bogni A, et al. Association between [18F]fluorodeoxyglucose uptake and postoperative histopathology, hormone receptor status, thymidine labelling index and p53 in primary breast cancer: a preliminary observation. Eur J Nucl Med. 1998; 25(10):1429–34. [PubMed: 9818284]

13. Bos R, van Der Hoeven JJ, van Der Wall E, van Der Groep P, van Diest PJ, Comans EF, et al. Biologic correlates of (18)fluorodeoxyglucose uptake in human breast cancer measured by positron emission tomography. J Clin Oncol. 2002; 20(2):379–87. [PubMed: 11786564]

14. Scheepers A, Joost HG, Schurmann A. The glucose transporter families SGLT and GLUT: molecular basis of normal and aberrant function. JPEN J Parenter Enteral Nutr. 2004; 28(5):364–71. [PubMed: 15449578]

15. Bormans GM, Van Oosterwyck G, De Groot TJ, Veyhl M, Mortelmans L, Verbruggen AM, et al. Synthesis and biologic evaluation of (11)c-methyl-d-glucoside, a tracer of the sodium-dependent glucose transporters. J Nucl Med. 2003; 44(7):1075–81. [PubMed: 12843224]

16. Brown RS, Goodman TM, Zasadny KR, Greenson JK, Wahl RL. Expression of hexokinase II and Glut-1 in untreated human breast cancer. Nucl Med Biol. 2002; 29(4):443–53. [PubMed: 12031879]

17. de Geus-Oei LF, van Krieken JH, Aliredjo RP, Krabbe PF, Frielink C, Verhagen AF, et al. Biological correlates of FDG uptake in non-small cell lung cancer. Lung Cancer. 2007; 55(1):79–87. [PubMed: 17046099]

18. Mamede M, Higashi T, Kitaichi M, Ishizu K, Ishimori T, Nakamoto Y, et al. [18F]FDG uptake and PCNA, Glut-1, and Hexokinase-II expressions in cancers and inflammatory lesions of the lung. Neoplasia. 2005; 7(4):369–79. [PubMed: 15967114]

19. Chung JK, Lee YJ, Kim SK, Jeong JM, Lee DS, Lee MC. Comparison of [18F]fluorodeoxyglucose uptake with glucose transporter-1 expression and proliferation rate in human glioma and non-small-cell lung cancer. Nucl Med Commun. 2004; 25(1):11–7. [PubMed: 15061260]

20. Marom EM, Aloia TA, Moore MB, Hara M, Herndon JE 2nd, Harpole DH Jr. et al. Correlation of FDG-PET imaging with Glut-1 and Glut-3 expression in early-stage non-small cell lung cancer. Lung Cancer. 2001; 33(2-3):99–107. [PubMed: 11551404]

21. Kurokawa T, Yoshida Y, Kawahara K, Tsuchida T, Okazawa H, Fujibayashi Y, et al. Expression of GLUT-1 glucose transfer, cellular proliferation activity and grade of tumor correlate with [F-18]-fluorodeoxyglucose uptake by positron emission tomography in epithelial tumors of the ovary. Int J Cancer. 2004; 109(6):926–32. [PubMed: 15027127]

22. Higashi T, Saga T, Nakamoto Y, Ishimori T, Mamede MH, Wada M, et al. Relationship between retention index in dual-phase (18)F-FDG PET, and hexokinase-II and glucose transporter-1 expression in pancreatic cancer. J Nucl Med. 2002; 43(2):173–80. [PubMed: 11850481]

23. Riedl CC, Akhurst T, Larson S, Stanziale SF, Tuorto S, Bhargava A, et al. 18F-FDG PET scanning correlates with tissue markers of poor prognosis and predicts mortality for patients after liver resection for colorectal metastases. J Nucl Med. 2007; 48(5):771–5. [PubMed: 17475966]

24. Paudyal B, Oriuchi N, Paudyal P, Higuchi T, Nakajima T, Endo K. Expression of glucose transporters and hexokinase II in cholangiocellular carcinoma compared using [18F]-2-fluro-2-deoxy-D-glucose positron emission tomography. Cancer Sci. 2008; 99(2):260–6. [PubMed: 18271924]

25. Tohma T, Okazumi S, Makino H, Cho A, Mochiduki R, Shuto K, et al. Relationship between glucose transporter, hexokinase and FDG-PET in esophageal cancer. Hepatogastroenterology. 2005; 52(62):486–90. [PubMed: 15816463]
26. Tian M, Zhang H, Higuchi T, Oriuchi N, Nakasone Y, Takata K, et al. Hexokinase-II expression in untreated oral squamous cell carcinoma: comparison with FDG PET imaging. Ann Nucl Med. 2005; 19(4):335–8. [PubMed: 16097646]
27. Dang CV, Semenza GL. Oncogenic alterations of metabolism. Trends in biochemical sciences. 1999; 24(2):68–72. [PubMed: 10098401]
28. DeBerardinis RJ, Lum JJ, Hatzivassiliou G, Thompson CB. The biology of cancer: metabolic reprogramming fuels cell growth and proliferation. Cell metabolism. 2008; 7(1):11–20. [PubMed: 18177721]
29. Vander Heiden MG, Cantley LC, Thompson CB. Understanding the Warburg effect: the metabolic requirements of cell proliferation. Science (New York, NY. 2009; 324(5930):1029–33.
30. Hsu PP, Sabatini DM. Cancer cell metabolism: Warburg and beyond. Cell. 2008; 134(5):703–7. [PubMed: 18775299]
31. Rathmell JC, Fox CJ, Plas DR, Hammerman PS, Cinalli RM, Thompson CB. Akt-directed glucose metabolism can prevent Bax conformation change and promote growth factor-independent survival. Molecular and cellular biology. 2003; 23(20):7315–28. [PubMed: 14517300]
32. Gordan JD, Thompson CB, Simon MC. HIF and c-Myc: sibling rivals for control of cancer cell metabolism and proliferation. Cancer cell. 2007; 12(2):108–13. [PubMed: 17692803]
33. Biaglow JE, Cerniglia G, Tuttle S, Bakanauskas V, Stevens C, McKenna G. Effect of oncogene transformation of rat embryo cells on cellular oxygen consumption and glycolysis. Biochemical and biophysical research communications. 1997; 235(3):739–42. [PubMed: 9207231]
34. Ramanathan A, Wang C, Schreiber SL. Perturbational profiling of a cell-line model of tumorigenesis by using metabolic measurements. Proceedings of the National Academy of Sciences of the United States of America. 2005; 102(17):5992–7. [PubMed: 15840712]
35. Sorlie T, Perou CM, Tibshirani R, Aas T, Geisler S, Johnsen H, et al. Gene expression patterns of breast carcinomas distinguish tumor subclasses with clinical implications. Proceedings of the National Academy of Sciences of the United States of America. 2001; 98(19):10869–74. [PubMed: 11553815]
36. Buck A, Schirrmeister H, Kuhn T, Shen C, Kalker T, Kotzerke J, et al. FDG uptake in breast cancer: correlation with biological and clinical prognostic parameters. Eur J Nucl Med Mol Imaging. 2002; 29(10):1317–23. [PubMed: 12271413]
37. Hanby AM, Hughes TA. In situ and invasive lobular neoplasia of the breast. Histopathology. 2008; 52(1):58–66. [PubMed: 18171417]
38. Specht JM, Kurland BF, Montgomery SK, Dunnwald LK, Doot RK, Gralow JR, et al. Tumor metabolism and blood flow as assessed by positron emission tomography varies by tumor subtype in locally advanced breast cancer. Clin Cancer Res. 16(10):2803–10. [PubMed: 20460489]
39. Basu S, Chen W, Tchou J, Mavi A, Cermik T, Czerniecki B, et al. Comparison of triple-negative and estrogen receptor-positive/progesterone receptor-positive/HER2-negative breast carcinoma using quantitative fluorine-18 fluorodeoxyglucose/positron emission tomography imaging parameters: a potentially useful method for disease characterization. Cancer. 2008; 112(5):995–1000. [PubMed: 18098228]
40. Gunther EJ, Belka GK, Wertheim GB, Wang J, Hartman JL, Boxer RB, et al. A novel doxycycline-inducible system for the transgenic analysis of mammary gland biology. Faseb J. 2002; 16(3):283–92. [PubMed: 11874978]
41. Boxer RB, Stairs DB, Dugan KD, Notarfrancesco KL, Portocarrero CP, Keister BA, et al. Isoform-specific requirement for Akt1 in the developmental regulation of cellular metabolism during lactation. Cell metabolism. 2006; 4(6):475–90. [PubMed: 17141631]
42. Boxer RB, Jang JW, Sintasath L, Chodosh LA. Lack of sustained regression of c-MYC-induced mammary adenocarcinomas following brief or prolonged MYC inactivation. Cancer cell. 2004; 6(6):577–86. [PubMed: 15607962]

43. Gunther EJ, Moody SE, Belka GK, Hahn KT, Innocent N, Dugan KD, et al. Impact of p53 loss on reversal and recurrence of conditional Wnt-induced tumorigenesis. Genes Dev. 2003; 17(4):488–501. [PubMed: 12600942]
44. Moody SE, Sarkisian CJ, Hahn KT, Gunther EJ, Pickup S, Dugan KD, et al. Conditional activation of Neu in the mammary epithelium of transgenic mice results in reversible pulmonary metastasis. Cancer cell. 2002; 2(6):451–61. [PubMed: 12498714]
45. Sarkisian CJ, Keister BA, Stairs DB, Boxer RB, Moody SE, Chodosh LA. Dose-dependent oncogene-induced senescence in vivo and its evasion during mammary tumorigenesis. Nat Cell Biol. 2007; 9(5):493–505. [PubMed: 17450133]
46. Minn AJ, Gupta GP, Siegel PM, Bos PD, Shu W, Giri DD, et al. Genes that mediate breast cancer metastasis to lung. Nature. 2005; 436(7050):518–24. [PubMed: 16049480]
47. Surti S, Karp JS, Perkins AE, Cardi CA, Daube-Witherspoon ME, Kuhn A, et al. Imaging performance of A-PET: a small animal PET camera. IEEE transactions on medical imaging. 2005; 24(7):844–52. [PubMed: 16011313]
48. Surti S, Karp JS, Perkins AE, Freifelder R, Muehllehner G. Design Evaluation of A-PET: A High Sensitivity Animal PET Camera. IEEE transactions on nuclear science. 2003; 50(5):1357–63.
49. Daube-Witherspoon M, Matej S, Karp J, Lewitt R. Application of the row action maximum likelihood algorithm with spherical basis functions to clinical PET imaging. IEEE Trans Nucl Sci. 2001; 48:24–30.
50. Zhao Y, Wieman HL, Jacobs SR, Rathmell JC. Mechanisms and methods in glucose metabolism and cell death. Methods in enzymology. 2008; 442:439–57. [PubMed: 18662583]
51. Model F, Adorjan P, Olek A, Piepenbrock C. Feature selection for DNA methylation based cancer classification. Bioinformatics. 2001; 17(Suppl 1):S157–64. [PubMed: 11473005]
52. D'Cruz CM, Gunther EJ, Boxer RB, Hartman JL, Sintasath L, Moody SE, et al. c-MYC induces mammary tumorigenesis by means of a preferred pathway involving spontaneous Kras2 mutations. Nature medicine. 2001; 7(2):235–9.
53. Ben-Haim S, Ell P. 18F-FDG PET and PET/CT in the evaluation of cancer treatment response. J Nucl Med. 2009; 50(1):88–99. [PubMed: 19139187]
54. Bryant KL, Mancias JD, Kimmelman AC, Der CJ. KRAS: feeding pancreatic cancer proliferation. Trends in biochemical sciences. 2014; 39(2):91–100. [PubMed: 24388967]

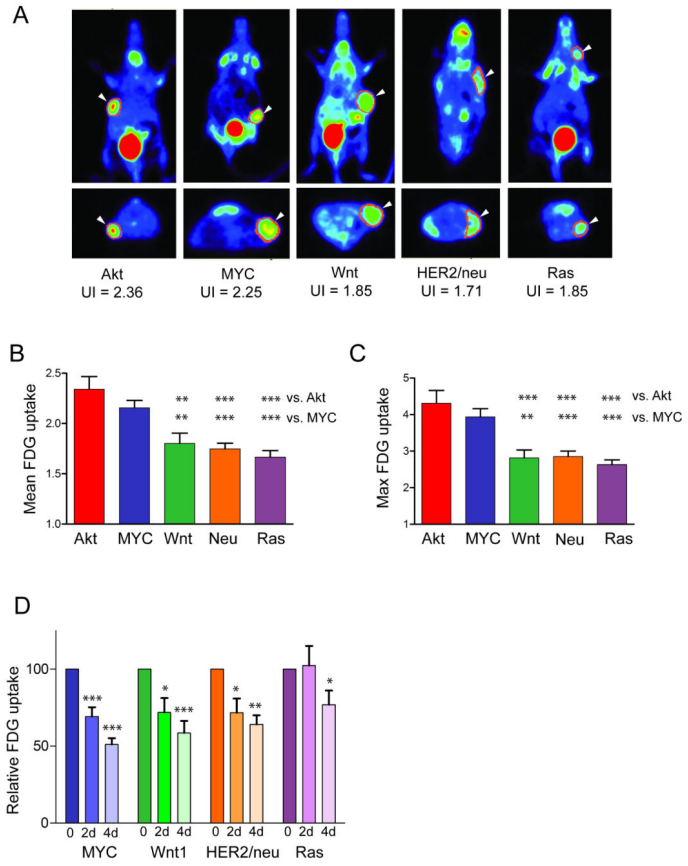

Figure 1. Oncogene-specific regulation of FDG uptake in mouse mammary tumors

A. Representative PET images of mammary tumors of the indicated genotype. Top panel: coronal view; Bottom panel: transverse view. B. Mean and C. Max FDG uptake for each tumor was expressed as an uptake index (UI). The average UI was calculated for each genotype and expressed as mean ± SEM. The variation in uptake between tumors of different genotypes was significant (ANOVA, $p<0.0001$), and Akt and Myc-driven tumors exhibited higher uptake than Wnt1, HER2/neu, or Ras-driven tumors. D. Mice were imaged in the presence of oncogene expression (Baseline) and 2 and 4 days following oncogene down-regulation. * $p<0.05$, ** $p<0.01$, *** $p<0.001$

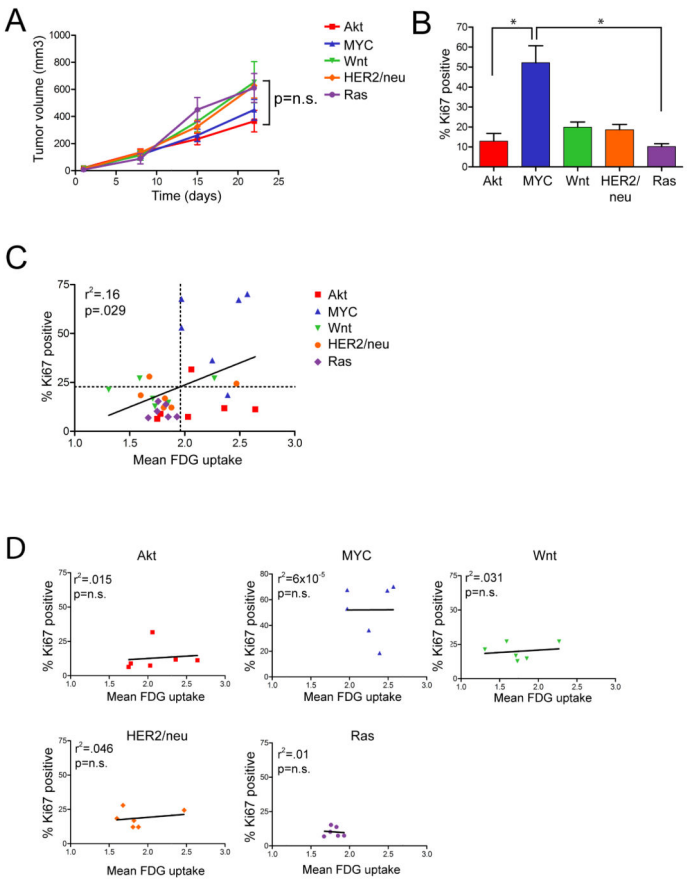

Figure 2. Tumor growth and cellular proliferation are not independent predictors of FDG uptake

A. Growth curves for tumors of the indicated genotype. There was no significant difference in the growth rates of tumors based on their genotypes. B. The proliferative rates of tumors were assessed by Ki67 staining. Proliferation rates varied significantly across genotypes (p=0.0011, Kruskal-Wallis test). C and D. Correlation between tumor cell proliferation and FDG uptake across all tumors (C) or within tumors of a given genotype (D). While there was a modest correlation between proliferation and FDG uptake, this correlation was dependent of the tumor's genotype, suggesting that proliferation is not an independent predictor of high uptake. *p<0.05

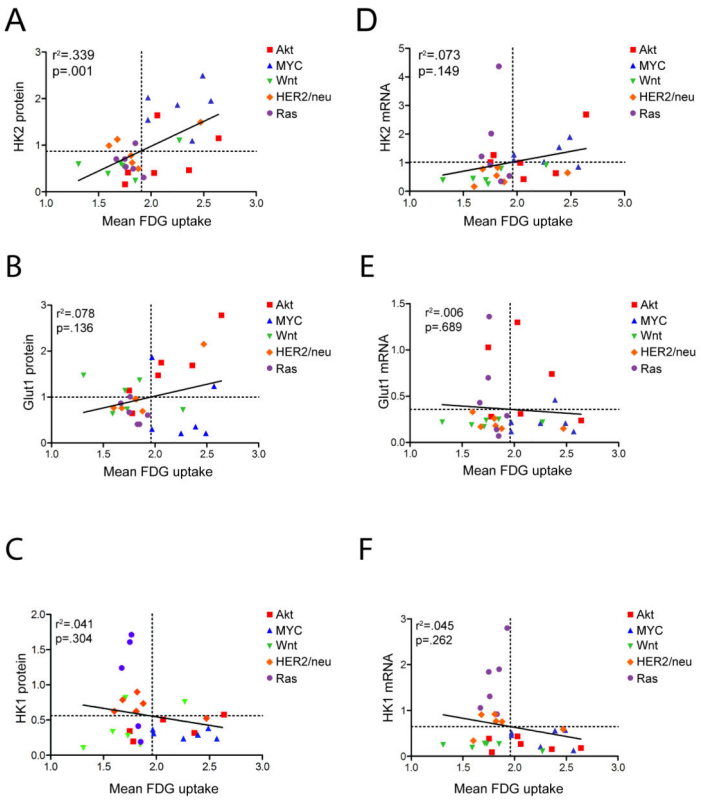

Figure 3. Expression of HK2 protein, but not Glut1 or HK1, is strongly correlated with FDG uptake

Correlation between FDG uptake and the protein (A-C) or mRNA (D-F) levels of HK2 (A, D), Glut1 (B, E), or HK1 (C, F). Only HK2 protein showed a significant correlation with FDG uptake across all tumors.

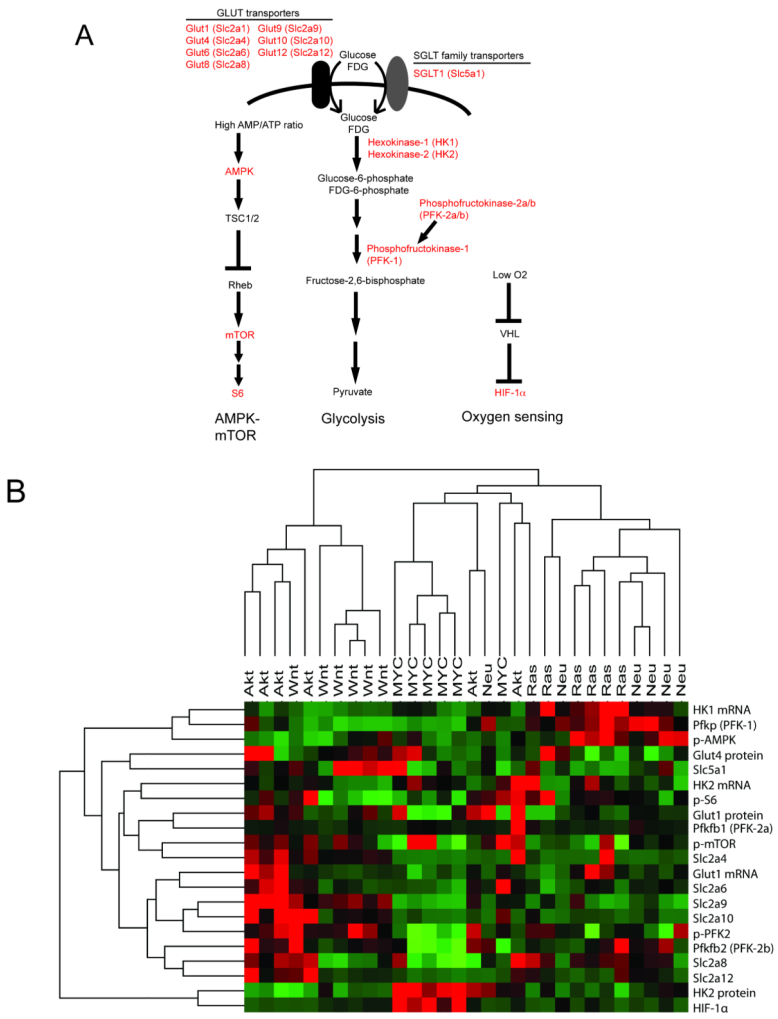

Figure 4. Quantitative analysis of glycolytic, energy- and oxygen-sensing pathways in mammary tumors

A. Pathways that regulate glucose metabolism and energy and oxygen sensing; the genes or proteins whose expression or phosphorylation was measured are shown in red. B. Expression or activation status of each gene or protein across 30 tumors from 5 genotypes was measured by qRT-PCR or quantitative western blotting. High values are shown in red, low values are shown in green. Tumors were grouped by unsupervised hierarchical clustering, and tumors of different genotypes were largely separated into distinct groups.

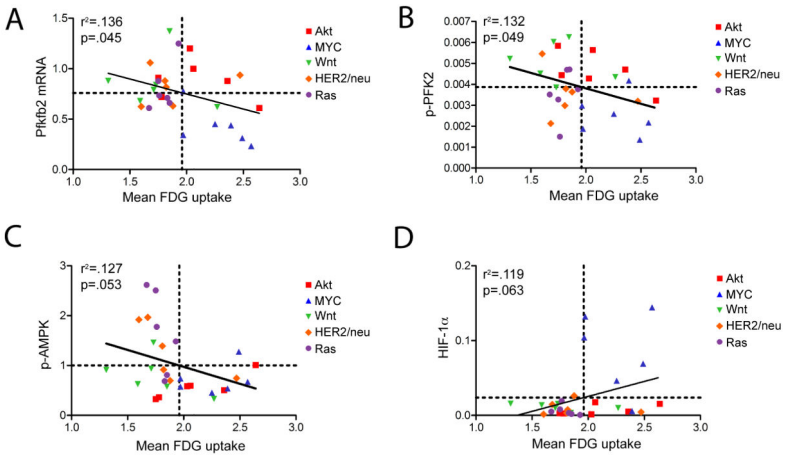

Figure 5. Molecular correlates of FDG uptake

FDG uptake is negatively correlated with PFK-2b mRNA (A), p-PFK2 (B), and activation of AMPK (C), and positively correlated with HIF-1α expression (D).

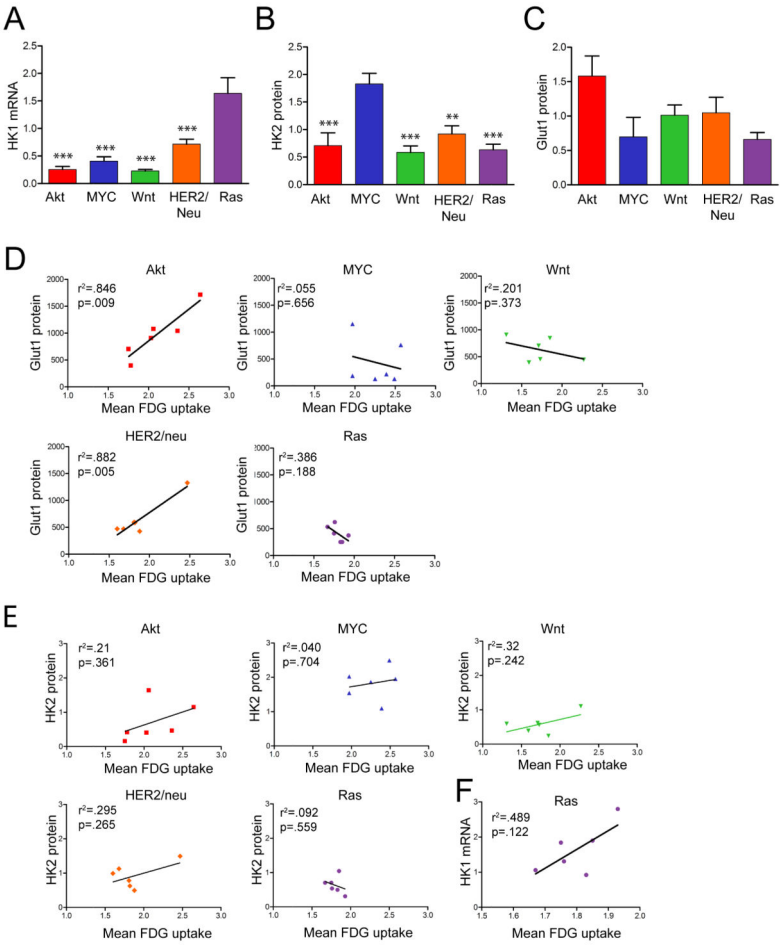

Figure 6. Oncogene-specific correlates of FDG uptake

A-C. HK1 (A), HK2 (B), and Glut1 (C) expression in tumors of the indicated genotype. Asterisks denote significant differences relative to Ras tumors in (A) and Myc tumors in (B). * $p<0.05$, ** $p<0.01$, *** $p<0.001$. D. Glut1 expression is associated with high FDG uptake in Akt- and HER2/neu-driven tumors, but not tumors of other genotypes. E. HK2 expression is not correlated with FDG uptake within tumors of the same genotype, though MYC-driven tumors have high HK2 expression and high uptake. F. Ras-driven tumors, but not tumors of other genotypes (data not shown), exhibit a strong correlation between FDG uptake and HK1 expression.

Table 1

Pearson correlation coefficients were measured between each gene or protein and FDG uptake in 30 tumors, irrespective of genotype (All tumors), or within the 6 tumors of each indicated genotype (Within genotype). Correlations that are statistically significant ($p<0.05$) are shown in red, and correlations that are marginally significant ($p<0.1$) are in bold.

Gene/Protein	All tumors	Within genotype				
		Akt	Myc	Wnt	Ras	Neu
Glut1 mRNA	−0.077	−0.323	0.166	0.227	−0.426	−0.562
Glut1 protein	0.276	**0.920**	−0.244	−0.447	−0.613	**0.942**
HK1 mRNA	−0.210	−0.315	−0.302	−0.602	0.700	−0.077
HK2 mRNA	0.270	0.541	0.210	**0.759**	−0.080	0.256
HK2 protein	**0.585**	0.463	0.196	0.567	−0.299	0.549
Glut4 protein	0.119	0.311	−0.148	−0.556	0.190	0.414
p-mTOR	0.191	0.141	0.015	−0.194	−0.549	**0.754**
p-S6	0.185	0.136	0.238	0.115	0.234	0.622
p-AMPK	− **0.355**	**0.879**	0.332	−0.490	−0.719	−0.693
PFK-1 mRNA	−0.176	−0.131	0.226	0.693	−0.199	0.224
PFK-2a mRNA	**0.385**	**0.733**	0.086	−0.151	0.041	−0.051
PFK-2b mRNA	**−0.369**	−0.363	−0.666	−0.116	0.674	0.273
Slc2a4 (Glut4)	−0.025	0.373	−0.117	**−0.814**	−0.261	−0.130
Slc5a1 (SLGT1)	**−0.415**	−0.582	−0.583	− **0.788**	0.161	0.263
Slc2a9 (Glut9)	−0.149	−0.373	0.228	0.173	−0.564	0.292
Slc2a8 (Glut8)	−0.163	0.137	−0.680	0.059	0.389	0.004
Slc2a10 (Glut10)	−0.180	− **0.790**	0.252	0.001	−0.131	−0.124
Slc2a12 (Glut12)	−0.089	−0.436	−0.719	0.140	**0.847**	−0.327
Slc2a6 (Glut6)	0.059	−0.453	0.129	−0.012	−0.472	−0.159
p-PFK2b	**−0.363**	−0.677	−0.087	−0.167	0.402	−0.252
Proliferation (% Ki67+)	**0.401**	0.130	0.002	0.173	−0.097	0.222
HIF-1α	**0.344**	0.564	−0.210	−0.522	−0.472	−0.089